A Compact Planar Omnidirectional MIMO Array Antenna With Pattern Phase Diversity Using Folded Dipole Element

Libin Sun, Yue Li, *Senior Member, IEEE*, Zhijun Zhang, *Fellow, IEEE*, and Magdy F. Iskander, *Life Fellow, IEEE*

***Abstract*— This paper presents a planar omnidirectional multiple-input multiple-output (MIMO) antenna with pattern phase diversity. The profiles of conventional dual-polarized omnidirectional MIMO antennas are too high to be planar integrated due to the limited bandwidth of vertical-polarized element. Therefore, a dual-channel horizontal-polarized MIMO antenna is proposed for the planar integration of omnidirectional MIMO antenna. The antenna is formed with four-element folded dipole array, and a compact feed network with two sets of 90° progressive phases is employed to feed the two channels with shared elements, thus the antenna can be integrated into a sheet of substrate with an ultralow profile of 0.8 mm. Although the polarization and radiation pattern (amplitude) of the two colocated channels are the same with each other, a high isolation is still achieved as a result of the orthogonal pattern phase. A prototype was fabricated to validate the performance. The measured highest isolation between two channels is 31.7 dB, and −10 dB isolated bandwidth is 2.29–2.57 GHz (11.7%) with $S_{11} < -14$ dB and envelope correlation coefficient less than 0.05, which shows a good diversity performance. Therefore, the proposed dual-channel antenna gives a feasible solution for the planar integration of the omnidirectional MIMO system.**

***Index Terms*— Antenna diversity, antenna radiation patterns, multiple-input multiple-output (MIMO), pattern phase diversity, planar integration.**

I. Introduction

In RECENT years, dual-polarized antennas are widely employed in multiple-input multiple-output (MIMO) systems to enhance the channel capacity [1]. In addition, omnidirectional pattern antennas have received great attention in some wireless communication systems such as the wireless local area networks and base stations. Therefore, many researchers focused on the dual-polarized antennas with omnidirectional patterns [2]–[14]. In [2]–[5], some wideband or multiband dual-polarized omnidirectional antennas are proposed with the circular dipole array for horizontal polarization (HP) and the discone antenna for vertical polarization (VP). An artificial magnetic conductor reflector is appended in [9] to reduce the profile of the structure in [3]. In [6] and [7], the cross bow-tie dipole is utilized for HP, while the inverted-cone antenna is utilized for VP. In [10] and [11], the vertical and horizontal slots are combined for the HP and VP, respectively. A novel sabre-like structure is proposed in [12] for the compactness of the dual-polarized antenna with the resonant cavity for HP and declining monopole for VP. The aforementioned antennas in [2]–[12] are all 3-D structures with high profiles, and it is hard for them to be integrated into a planar platform. To satisfy the requirement of planar integration, some planar dual-polarized omnidirectional MIMO antennas are presented in [13] and [14]. However, the bandwidths of them are narrow owing to the intrinsic narrowband property of the low-profile omnidirectional VP element. To solve this problem, a planar dual-channel HP omnidirectional MIMO antenna is proposed in this paper. Because the two channels are both HP, the bandwidth of the proposed antenna will not be limited. The high isolation between two copolarization channels is achieved by a pattern phase diversity technique.

In traditional MIMO systems, polarization diversity [2]–[14], spatial diversity [15]–[19], and radiation pattern diversity [20]–[33] techniques are exploited to enhance the port isolations between multiple channels. In polarization diversity, two orthogonal polarizations are utilized to decoupling between two channels. In spatial diversity, parasitic structures [15], slot etching [16], electromagnetic bandgap structures [17], and neutralization lines [18], [19] are applied to reduce the mutual coupling with closely spaced elements. In radiation pattern diversity, there are three different ways to decoupling between multiple channels. The first way is employing different modes of patch antenna to generate broadside and conical radiation patterns [20]–[26]. This method can be realized in a single radiator and thus has a simple antenna structure. The second way is using different radiators to generate different beam-pointing patterns [27]–[30]. The third way is utilizing different feed phases for the antenna array to achieve different radiation patterns [31], [32]. The above-mentioned pattern diversity

Manuscript received September 27, 2018; revised November 14, 2018; accepted December 4, 2018. Date of publication December 24, 2018; date of current version March 5, 2019. This work was supported in part by the National Natural Science Foundation of China under Contract 61525104 and Contract 61771280 and in part by the Beijing Natural Science Foundation under Contract 4182029. *(Corresponding author: Zhijun Zhang.)*

L. Sun, Y. Li, and Z. Zhang are with the Beijing National Research Center for Information Science and Technology, Tsinghua University, Beijing, 100084, China (e-mail: zjzh@tsinghua.edu.cn).

M. F. Iskander is with the Hawaii Center for Advanced Communications, University of Hawai'i at Mānoa, Honolulu, HI 96822 USA (e-mail: magdy.iskander@gmail.com).

Color versions of one or more of the figures in this paper are available online at http://ieeexplore.ieee.org.

Digital Object Identifier 10.1109/TAP.2018.2889608

techniques proposed in [20]–[32] are all based on the amplitude diversity of the radiation patterns, but cannot generate two isolated omnidirectional radiation channels. To decoupling in the same polarization and beam pointing, a pattern phase diversity technique is exploited in this paper to achieve a high isolation between two shared-aperture channels.

Except the dual-polarized omnidirectional antenna, some co-VP omnidirectional antennas are proposed in the full-duplex systems [33]–[36]. A VP progressively phased circular array used in antenna isolation is first proposed in 1974 [33]. There are two isolated channels in [33], one channel is a progressively phased four-element circular dipole array, and another channel is a single dipole placed at the center of the circular array, which is the electric field null of the first channel, thus a high isolation can be acquired between them. To avoid affecting the omnidirectional radiation pattern of the inner element, the inner element is placed in a higher step in [34]. The inner element can also be replaced by the progressively phased circular array, thus two progressively phased circular arrays with different feed phases are proposed in [35]. An improved broadband version is presented in [36]. The aforementioned research studies [33]–[36] are all dual-channel omnidirectional antennas, but the transmit and receive antennas are not shared-aperture and the profiles are too high to be planar integrated.

To achieve a planar omnidirectional MIMO antenna with adequate bandwidth, a co-HP omnidirectional MIMO antenna is proposed for the first time in this paper. Four-element planar folded dipole array is fed in two different progressive phases to achieve two isolated channels, and identical HP omnidirectional patterns for both channels are obtained. The high isolation between two channels is achieved by the orthogonal pattern phase distribution in the azimuth plane. In addition, a compact feed network is placed in the center of the planar folded dipole array to integrate the whole antenna system in a single sheet of substrate. Therefore, the profile of the proposed omnidirectional MIMO antenna can be reduced to 0.8 mm ($0.006\lambda_0$) and easy to be planar integrated. Compared with the traditional dual-polarized planar omnidirectional MIMO antenna [13], [14], the narrowband problem can be solved for the absence of VP channel. Consequently, a planar omnidirectional MIMO antenna with adequate bandwidth is realized by a pattern phase diversity technique.

This paper is organized as follows. In Section II, the theorical analysis of the pattern phase diversity technique is discussed; besides, the antenna structure and evolution process are discussed. In Section III, the designs of the proposed antenna and feed network are presented with parameter analysis. In Section IV, the antenna fabrication and measurement results are shown, and a comparison chart is reported to highlight the merits. Finally, Section V draws a conclusion of this paper.

II. Principle Analysis

A. Theory Analysis of the Pattern Phase Diversity

In a MIMO system, the communication capacity can be enhanced if the antenna elements are weakly correlated, thus the goal of the MIMO antenna is to reduce the correlation between every channel. The envelope correlation coefficient (ECC) is a significant parameter to evaluate the correlation between two channels, and it can be calculated by the complex radiated far field, the formulation is shown as follows [37]:

$$\rho_e \approx |\rho_c|^2 = \left| \frac{\iint A_{12}(\theta,\varphi)\sin\theta \mathrm{d}\theta\mathrm{d}\varphi}{\iint A_{11}(\theta,\varphi)\sin\theta \mathrm{d}\theta\mathrm{d}\varphi \cdot \iint A_{22}(\theta,\varphi)\sin\theta \mathrm{d}\theta\mathrm{d}\varphi} \right|^2 \quad (1)$$

where

$$A_{ij} = E_{\theta,i}(\theta,\varphi)\cdot E^*_{\theta,j}(\theta,\varphi) + E_{\varphi,i}(\theta,\varphi)\cdot E^*_{\varphi,j}(\theta,\varphi). \quad (2)$$

Here, $E_{\theta,i}$ and $E_{\varphi,i}$ are the complex electric field of channel i in the elevation and azimuth planes, respectively. $()*$ is the conjugate operator.

Two different phase distributions of the far field with omnidirectional radiation pattern in the azimuth plane are illustrated in Fig. 1. As shown in Fig. 1(a), the phase increases from 0 to 2π with φ increased, let us define it as $+1$ mode. As for Fig. 1(b), the phase decreases from 2π to 0 with φ increased, and let us define it as -1 mode. Note that the polarizations and radiation beams of these two modes are identical to each other. To quantitatively evaluate the diversity performance of the pattern phase diversity technique, the ECC between these two modes is calculated. If only considering the complex electric field in the azimuth plane, (1) can be simplified as

$$\rho_e \approx |\rho_c|^2 = \left| \frac{\int_0^{2\pi} A_{12}(\varphi)\mathrm{d}\varphi}{\int_0^{2\pi} A_{11}(\varphi)\mathrm{d}\varphi \cdot \int_0^{2\pi} A_{22}(\varphi)\mathrm{d}\varphi} \right|^2 \quad (3)$$

where

$$A_{ij}(\varphi) = E_{\varphi,i}(\varphi)\cdot E^*_{\varphi,j}(\varphi). \quad (4)$$

The complex electric field in Fig. 1(a) and (b) can be expressed as

$$E_{\varphi,1}(\varphi) = e^{j\varphi} \quad (5)$$

$$E_{\varphi,2}(\varphi) = e^{-j\varphi}. \quad (6)$$

If we substitute the complex electric field in (5) and (6) into (3), we get

$$\int_0^{2\pi} A_{12}(\varphi)\, d\varphi = \int_0^{2\pi} e^{2j\varphi} d\varphi = 0. \quad (7)$$

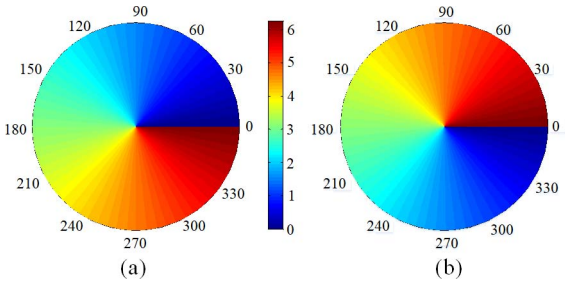

Fig. 1. Two different phase distributions of the omnidirectional radiation pattern in the azimuth plane (normalized by the phase at $\varphi = 0°$). (a) Increasing phase distribution ($+1$ mode). (b) Decreasing phase distribution (-1 mode).

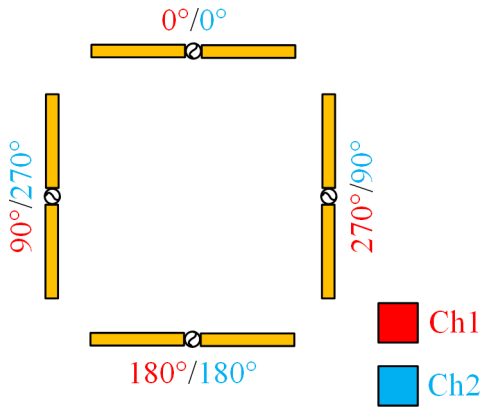

Fig. 2. Schematic of the dual-channel four-element planar dipole array excited with 90° and −90° progressively phase.

Therefore, two uncorrelated channels are realized by the pattern phase diversity technique.

B. Antenna Structure

The conventional strategy to achieve HP omnidirectional radiation pattern is employing the dipole array to generate a zero-order loop mode with in-phase currents [2]–[5], which can be equivalent to the radiation of magnetic current. However, the pattern phase of the zero-order loop is kept unchanged in the azimuth plane, thus it is inappropriate for the pattern phase diversity technique. Different from the zero-order loop mode dipole array, a four-element planar dipole array excited with 90° and −90° progressively phase is proposed to achieve the HP omnidirectional pattern, as shown in Fig. 2. For the MIMO channel 1 (Ch1), the excited phase is anticlockwise 90° progressive phase (defined as +1 mode), the far-field phase is just like that in Fig. 1(a). While for the MIMO channel 2 (Ch2), the excited phase is clockwise 90° progressive phase (defined as −1 mode), which is just like that in Fig. 1(b). Although the two channels share the same four-element dipole array, a high isolation with the pattern phase diversity technique can be achieved.

In order to avoid confusion, it should be noted that the proposed dipole array is totally different from the sequentially rotated array (SRA) in [38] for the circularly polarization (CP). The difference between them is illustrated in Fig. 3. As can be seen in Fig. 3(a), the current directions of the opposite dipoles are inverse. While for the SRA, although the feed phase is defined as 0° and 180° for the upper and lower dipoles, the currents of them are in the same direction as shown in Fig. 3(b). Because for the SRA, the dipole elements and feed phase are both sequentially rotated, thus the superposition of those two inverse phases contributes to the same current direction for the opposite elements. Therefore, the radiation pattern of the proposed dipole array is an omnidirectional pattern in the azimuth plane and has a null in the broadside as shown in Fig. 3(c), while the SRA creates a bidirectional CP radiation pattern as shown in Fig. 3(d).

The mechanism of the omnidirectional radiation pattern of the proposed dipole array is explained in Fig. 4 by a variation of the classical turnstile antenna [39]. For a vertical

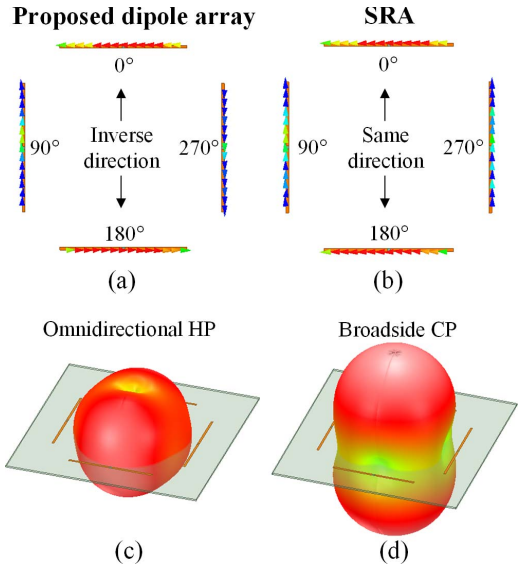

Fig. 3. Difference between the proposed dipole array and the sequentially rotated CP array. (a) Vector current distribution of the proposed dipole with +1 mode excited. (b) Vector current distribution of the SRA. (c) Radiation pattern of the proposed dipole with +1 mode excited. (d) Radiation pattern of the SRA.

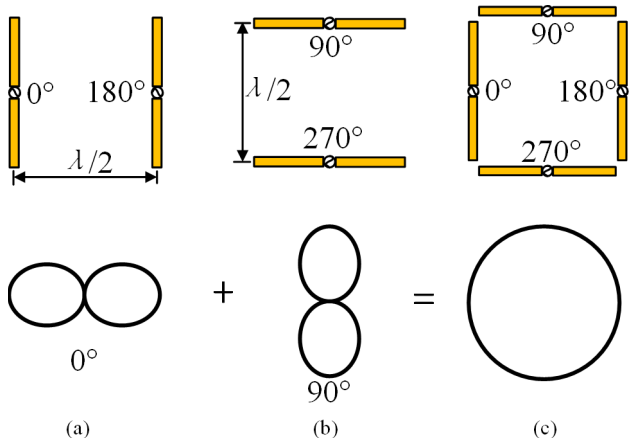

Fig. 4. Schematic of the radiation patterns for the proposed dipole array by a variation of the turnstile antenna.

arranged dual-element dipole array fed by equal amplitude but opposite phase, the radiation pattern can be deduced by the pattern multiplication theory as shown in Fig. 4(a). Similarly, the radiation pattern of the horizontal arranged dipole array with opposite phase excited is an "eight-" shaped pattern as shown in Fig. 4(b). Then, if we combine the horizontal and vertical arranged dual-element dipole arrays and add a 90° phase shift between them, the 90° progressively phased four-element dipole array comes into being as shown in Fig. 4(c). The radiation pattern of the proposed four-element dipole array can be derived by the superposition of the radiation patterns in Fig. 4(a) and (b) with a 90° phase shift. An omnidirectional radiation pattern with HP can be achieved according to the theory of the turnstile antenna [39]. However, the radiation pattern of the dual-element dipole array is slightly sharper than a single dipole, thus the pattern of the proposed four-element turnstile antenna is not a perfect omnidirection as an ideal turnstile antenna.

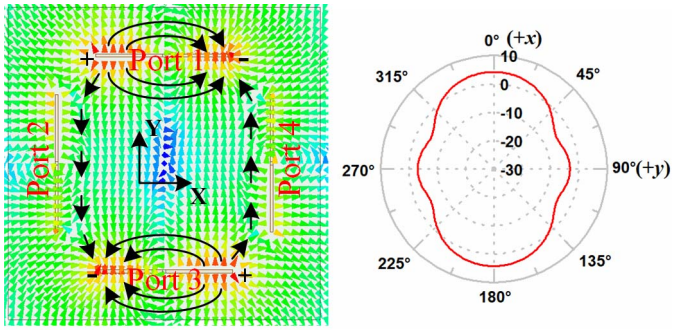

Fig. 5. Vector electric field distribution of the four-element straight dipole array and corresponding radiation pattern (dipole length 43 mm and element distance 70 mm). (a) Electric field distribution with ports 1 and 3 excited with equal amplitude but opposite phase. (b) Corresponding radiation pattern.

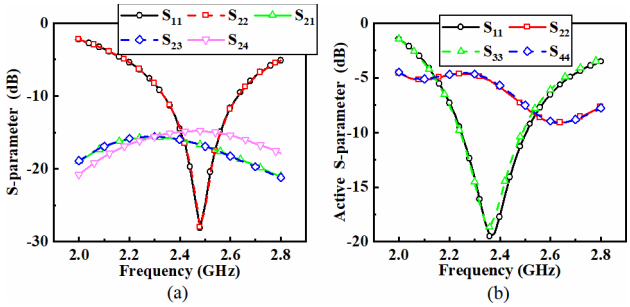

Fig. 6. Passive and active S-parameters of the antenna in Fig. 5. (a) S-parameter. (b) Active S-parameter.

C. Antenna Evolution

However, the aforementioned 90° progressively phase four-element straight dipole array does not work as proposed due to the mutual coupling between the neighboring elements, the mechanism is illustrated in Fig. 5(a). If ports 1 and 3 are excited with equal amplitude but opposite phase while ports 2 and 4 are matched, the electric fields of those two excited dipoles are inverse with each other. The inverse electric fields of the excited dipoles, which serves as a differential pair, will sustain the existence of the electric fields along the y-axis, thus the energy will be coupled to the two parasitic dipoles. The mutual coupling between the neighboring elements will deteriorate the active S-parameters of the elements. The S-parameter and active S-parameter of the proposed four-element straight dipole array are shown in Fig. 6. Although the isolations between those dipole elements are better than 15 dB as shown in Fig. 6(a), the active S-parameters of ports 1 and 2 (or ports 3 and 4) are totally different with severely deteriorations of ports 2 and 4. As we all know, the active S-parameter of a four-port network can be written as follows:

$$\text{Active } S_{mm} = S_{m1} \cdot \frac{a_1}{a_m} + S_{m2} \cdot \frac{a_2}{a_m} + S_{m3} \cdot \frac{a_3}{a_m} + S_{m4} \cdot \frac{a_4}{a_m} \tag{8}$$

where a_1–a_4 are the complex excited signals of the ports 1–4. For port 2, the coupling signals from ports 1 and 3 are with equal amplitude and phase, thus the superposition of them will lead to a mutual-coupling increment of 6 dB (20 × lg2). Moreover, if we assume that S_{21}, S_{22}, S_{23}, and S_{24} are all

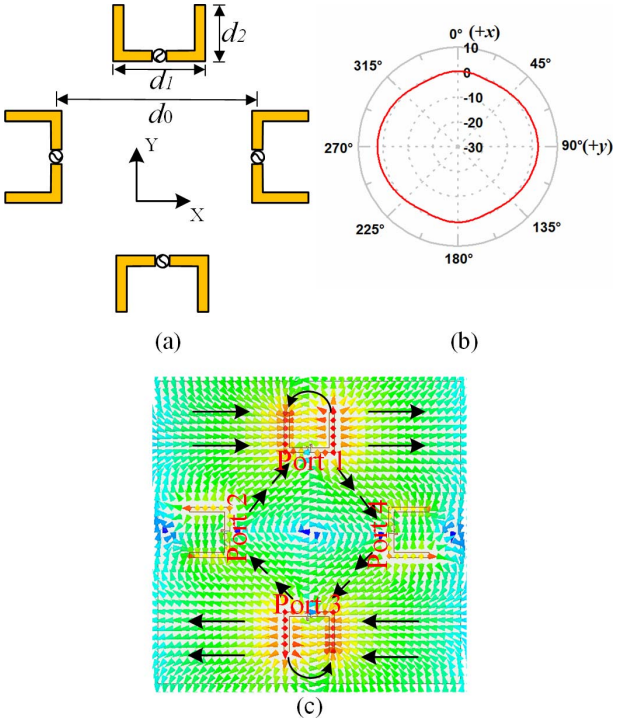

Fig. 7. Modified four-element folded dipole array and corresponding radiation pattern and vector electric field. (a) Proposed four-element folded dipole array (d_0 = 65 mm, d_1 = 20 mm, and d_2 = 16 mm). (b) Radiation pattern. (c) Electric field distribution with ports 1 and 3 excited with equal amplitude but opposite phase.

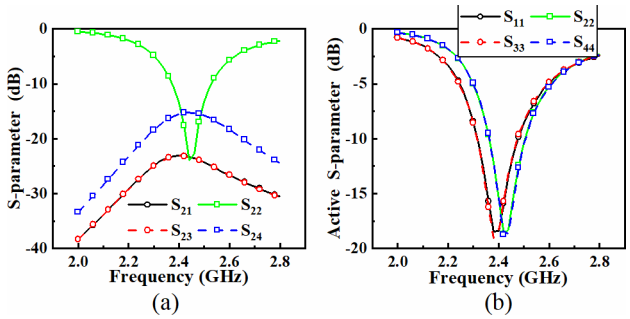

Fig. 8. Passive and active S-parameters of the proposed antenna in Fig. 7. (a) S-parameter. (b) Active S-parameter.

−15 dB and the phase of them are identical, the superposition of them will lead to an increment of 12 dB (20 × lg4) for the active S_{22}, i.e., it will be deteriorated from −15 to −3 dB in the worst case. That is the reason why a good S_{11} and isolation will lead to a deteriorated active S-parameter. Therefore, it is hard to achieve a similar active S-parameter for ports 1 and 2 (or ports 3 and 4) due to the asymmetric excited phase. Hence, the radiation pattern of the proposed structure is deteriorated as a result of different radiation powers of the horizontal and vertical dipole arrays as shown in Fig. 5(b).

In order to reduce the mutual coupling between the neighboring elements, a modified 90° progressively phase folded dipole array is proposed in Fig. 7(a). The vector electric field distribution when ports 1 and 3 are excited with equal amplitude but opposite phase is depicted in Fig. 7(c). The end points of the dipoles, which have the maximum electric field,

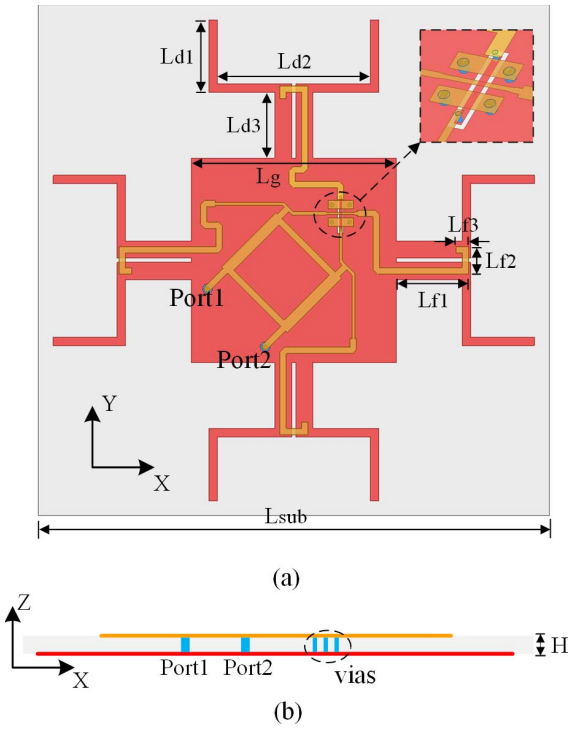

Fig. 9. Antenna structure of the proposed dual-channel planar folded dipole antenna array. (a) Top view. (b) Side view.

are separated apart from the neighboring dipoles to enhance the isolation. Moreover, the *E*-field of the folded dipole is changed, and it looks more like a cavity with three electric walls. Consequently, an enhanced isolation of better than 23 dB between the neighboring elements is obtained, as shown in Fig. 8(a), although the element distance d_0 is reduced from 70 to 65 mm. In addition, the phase of the S-parameter can be adjusted by the degree of folding (d_1 and d_2), thus the mutual coupling from different ports can be canceled out with an optimized phase. Accordingly, the enhanced isolation and optimized phase contribute to similar active S-parameters for the four ports as shown in Fig. 8(b). Therefore, an omnidirectional radiation pattern is acquired with the similar radiation powers of the horizontal and vertical dipoles as shown in Fig. 7(b).

III. Antenna Design

A. Antenna Configuration

The final structure of the proposed dual-channel planar folded dipole antenna array is shown in Fig. 9. A compact feed network is printed on the top side (in yellow) of the 0.8 mm thick FR-4 substrate ($\varepsilon_r = 4.4$, $\tan\delta = 0.02$), while the ground plane of the feed network and planar folded dipole array is printed on the back side (in red) of the FR-4 substrate. Thus, the whole antenna can be integrated into a single sheet of FR-4 board. The feed network is composed of a 3 dB coupler, a crossover, and four microstrip lines (MSLs). The crossover with MSL-conductor backed coplanar waveguide-MSL is shown in the enlarged inset, which can achieve a broadband transmission with low insertion loss and high isolation [40]. Four integrated baluns are employed to feed the four planar folded dipoles. The impedance match of dipoles

TABLE I
Detailed Dimensions (Unit: mm)

Parameter	L_{d1}	L_{d2}	L_{d3}	L_g	H
Value	17	36	15.5	48	0.8
Parameter	L_{f1}	L_{f2}	L_{f3}	L_{sub}	
Value	17	6.5	2.8	120	

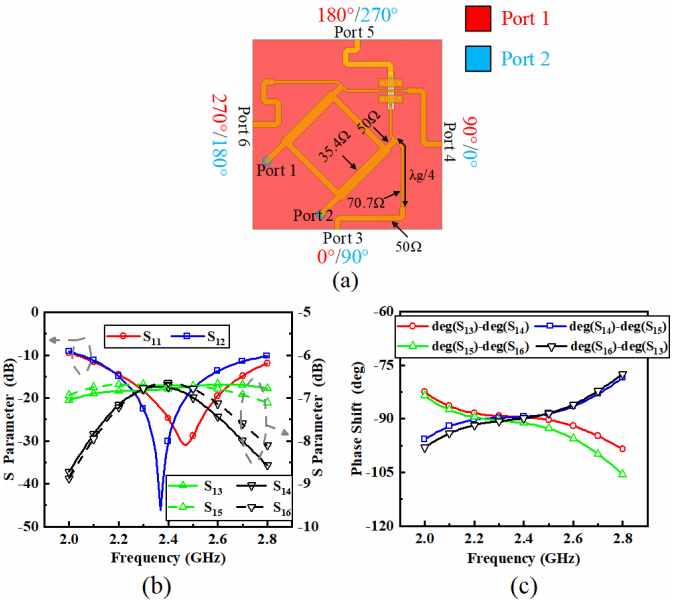

Fig. 10. Feed network and its simulated amplitude and phase characteristics. (a) Detailed feed network. (b) S-parameters of the feed network. (c) Phase shifts of the feed network.

can be tuned by the dimensions of L_{f1} and L_{f3}. The size of the ground plane should be small enough to avoid affecting the omnidirectional radiation pattern. The final dimensions of the proposed antenna are optimized by high-frequency structure simulator version 18.0, and the detailed dimensions are listed in Table I.

B. Integrated Feed Network

In order to avoid affecting the omnidirectional radiation pattern of the proposed antenna, a compact feed network with two sets of 90° progressively phases is designed to be integrated into the center of the dipole array as shown in Fig. 10(a). The proposed feed network has two input ports (ports 1 and 2) and four output ports (ports 3–6). Note that the integral lines of ports 3 and 5 (or ports 4 and 6) are inverse with each other due to the inverse baluns of the opposite elements, as shown in Fig. 9. The phases on output ports 3–6 when fed through port 1 are 0°, 90°, 180°, and 270°, while that of port 2 is 90°, 0°, 270°, and 180°. Therefore, two sets of orthogonal phased excitations, which can be employed in pattern phase diversity, are achieved. The amplitude characteristics of the feed network are shown in Fig. 10(b), and a good impedance match and isolation performance between two input ports are obtained. However, the impedance match, isolation, and transmission consistency

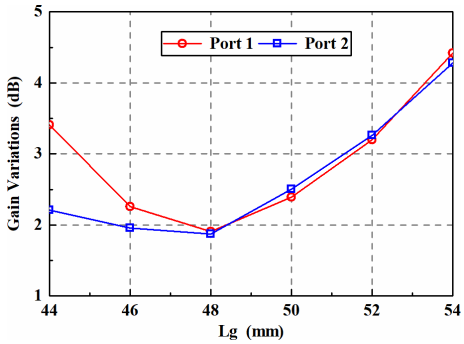

Fig. 11. Simulated gain variations in the azimuth plane at 2.4 GHz with the size of the ground plane L_g varied.

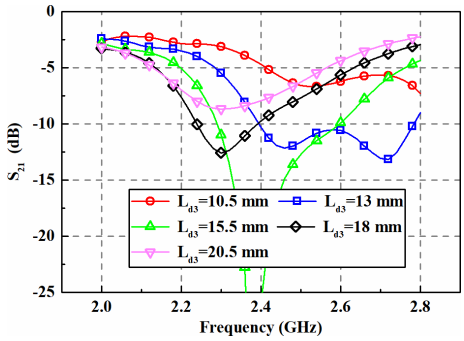

Fig. 12. S_{21} with the element distance L_{d3} varied.

between output ports of a single-order 3 dB coupler are narrow band, which limits the isolated bandwidth of the whole antenna system. The phase shifts between four output ports are shown in Fig. 10(c), and flat phase curves with phase variations less than 15° are observed across 2–2.8 GHz.

C. Parameter Analysis

The size of the ground plane L_g is an important parameter to adjust the omnidirectional radiation pattern. As shown in Fig. 11, the simulated gain variations at 2.4 GHz with L_g varied are analyzed. For both ports 1 and 2, two least gain variations are obtained with L_g optimized to 48 mm, and the gain variations deteriorate quickly with L_g increased. Therefore, in order to obtain a good omnidirectional radiation pattern, the size of the ground plane has to be reduced to an optimal dimension, which limits the design of the dual-channel 90° progressively phase feed network.

As mentioned before, the element distance is of great significance to the active impedance matching. A bad active impedance matching will reflect the energy from the dipole elements, leading to a bad isolation between two channels. The isolation between two channels with the element distance L_{d3} varied is analyzed in Fig. 12. The isolation deteriorates quickly with the element distance varied, and an optimal isolation is obtained with $L_{d3} = 15.5$ mm.

IV. Antenna Fabrication and Measurement Results

A. Antenna Fabrication

In order to validate the performance of the proposed dual-channel omnidirectional MIMO antenna, a prototype was

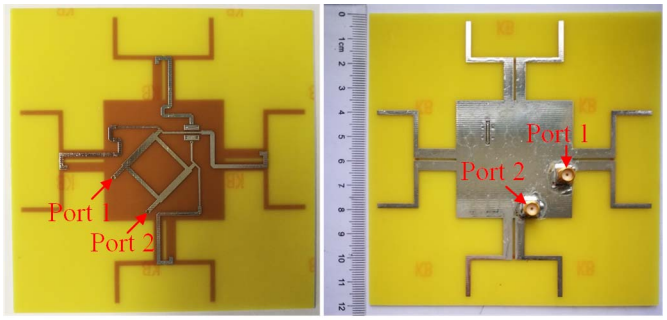

(a) (b)

Fig. 13. Photographs of the proposed antenna. (a) Front side. (b) Back side.

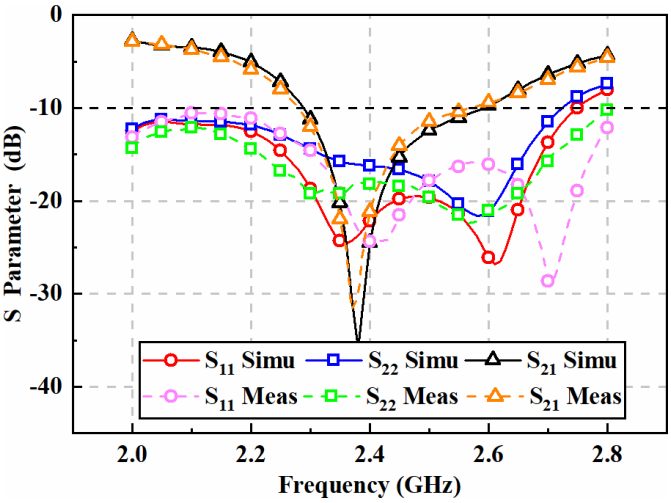

Fig. 14. Simulated and measured S-parameters of the proposed antenna.

fabricated by a single sheet of FR-4 substrate. The front and back sides of the proposed antenna are shown in Fig. 13(a) and (b), respectively. Two 50 Ω SMA connectors are soldered on the back side of the ground plane.

B. S-Parameters and Radiation Performance

The reflection coefficient and isolation between two channels are measured by an Agilent E5071B vector network analyzer (300 kHz–8.5 GHz). The simulated and measured results are shown in Fig. 14. The measured S_{11} and S_{22} are less than −10 dB across 2–2.8 GHz (33.3%). Small deviations between the measured and simulated results are occurred due to the fabrication error and impact of the SMA connectors. The measured and simulated isolations have good consistency, and the measured highest isolation is 31.7 dB at 2.37 GHz. The simulated and measured −10 dB S_{21} bandwidths are 2.29–2.59 GHz (12.5%) and 2.29–2.57 GHz (11.7%), respectively.

The radiation performance of the proposed antenna is measured in an anechoic chamber, and the simulated and measured normalized radiation patterns at 2.4 GHz are shown in Fig. 15. Two HP omnidirectional patterns in the azimuth plane (*xy*plane) for both channels are shown in Fig. 15(a) and (c). The simulated and measured gain variations in the azimuth plane fed by port 1 are less than 1.8 and 3.4 dB, while the simulated and measured results for port 2 are 2.0 and 2.5 dB,

TABLE II
COMPARISONS OF THE DIFFERENT OMNIDIRECTIONAL MIMO ANTENNAS

Ref.	Diversity Techniques	Structures	Profile	Size	Overlapping Bandwidths [a]	Gain Variation (Ch1/Ch2)	Efficiency (Ch1/Ch2)
[2]	Polarization	3D	0.18 λ_0 [b]	Φ0.78 λ_0	25%	2.5/1.5 dB	NG
[9]	Polarization	3D	0.22 λ_0	1.47×1.47 λ_0^2	45%	3.5/3 dB	~80%/~70%
[11]	Polarization	3D	0.34 λ_0	0.1×0.1 λ_0^2	4.1%	4.5/2.3 dB	78-95%/63-74%
[13]	Polarization	Planar (two sheets)	0.065 λ_0	Φ1.57 λ_0	5.9%	NG	NG
[14]	Polarization	Planar (two sheets)	0.057 λ_0	0.63×0.63 λ_0^2	3.7%	<1dB	NG
[33]	Radiation pattern phase (VP)	3D	~0.5 λ_0	Φ0.6 λ_0	NG	NG	NG
[34]	Radiation pattern phase (VP)	3D	>0.5 λ_0	>Φ0.5 λ_0	>36.7%	~5 dB	NG
[35]	Radiation pattern phase (VP)	3D	~2.55 λ_0	~Φ1.13λ_0	>94%	NG	NG
[36]	Radiation pattern phase (VP)	3D	0.74 λ_0	> Φ2.27 λ_0	98%	5/<5dB	47-82%/20-83%
Proposed	Radiation pattern phase (HP)	Planar (one sheet)	0.006 λ_0	0.96×0.96 λ_0^2	11.7%	3.4/2.5dB	50-73%/52-75%

[a] The overlapping bandwidth is the combined bandwidths of S_{11}<-10 dB, S_{22}<-10 dB, and S_{21}<-10 dB.
[b] λ_0 is the wavelength at the center frequency.

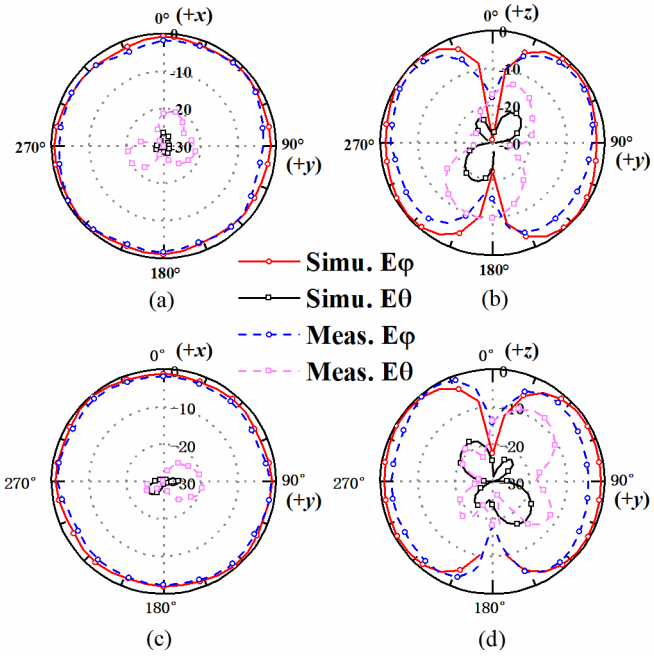

Fig. 15. Simulated and measured normalized radiation patterns of the proposed antenna at 2.4 GHz. (a) Port 1 in the *xy* plane. (b) Port 1 in the *yz* plane. (c) Port 2 in the *xy* plane. (d) Port 2 in the *yz* plane.

respectively. Therefore, good omnidirectional radiations for both channels are realized.

The simulated and measured total efficiencies are shown in Fig. 16. In the band of 2.3–2.6 GHz, the simulated efficiencies are 59%–73% and 59%–71% for ports 1 and 2, respectively, while the measured results are 50%–73% and 52%–75% for ports 1 and 2, respectively. There are small deviations between the simulated and measured results due

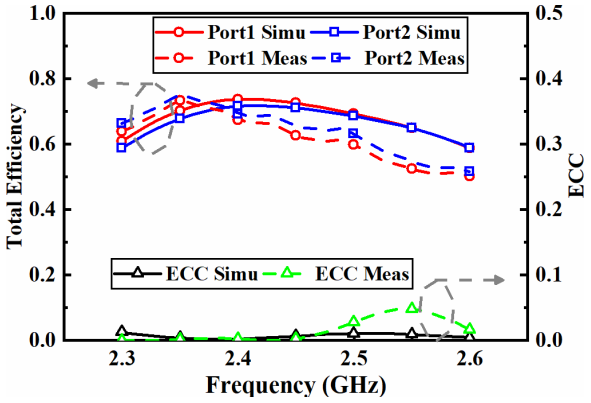

Fig. 16. Simulated and measured total efficiencies of the proposed antenna.

to the fabrication error and impact of the test connectors and cables. The loss of the FR-4 substrate contributes to the drop in radiation efficiency.

As discussed in Section II-A, the theoretic ECC between two orthogonal phased channels is 0 according to (3)–(7). To evaluate the diversity performance of the proposed antenna, the simulated and measured ECCs of the two channels are depicted in Fig. 16. A good orthogonality with measured ECC < 0.05 between two radiated far fields is achieved across the isolated band.

C. Discussion

In order to highlight the advantages of the proposed omnidirectional MIMO antenna, a comparison chart is listed in Table II. The proposed antenna is compared with various omnidirectional MIMO antennas. The typical way to design two isolated channels is utilizing the polarization

diversity technique. Most of them [2]–[12] are 3-D structure with high profile, and it is hard for them to be planar integrated. The planar omnidirectional MIMO antenna is proposed in [13] and [14]. However, the bandwidths of them are limited due to the narrow radiation aperture of the low-profile VP element. In [24], a wideband co-VP full-duplex antenna is proposed, and the pattern phase diversity technique is utilized to decoupling between two channels, but it has a high profile and large size. To achieve a planar-integrated MIMO antenna with adequate bandwidth, a co-HP dual-channel omnidirectional MIMO antenna is proposed in this paper with pattern phase diversity. The proposed antenna has an ultralow profile of 0.8 mm ($0.006\lambda_0$) and an adequate bandwidth of 11.7%.

V. Conclusion

A planar omnidirectional MIMO antenna with two HP channels is proposed in this paper. A radiation pattern phase diversity technique is utilized to decoupling between two channels with identical polarizations and radiation patterns (amplitude). The achieved impedance bandwidth for both of the channels is larger than 33.3%, and the isolated bandwidth between two channels is 11.7%. The simulated and measured ECCs between two channels are less than 0.05 across the isolated band, which shows a good diversity performance. Therefore, the proposed antenna paves the way for the planar integration of the omnidirectional MIMO antenna system.

References

[1] G. C. Raleigh and J. M. Cioffi, "Spatio-temporal coding for wireless communication," *IEEE Trans. Commun.*, vol. 46, no. 3, pp. 357–366, Mar. 1998.

[2] X. Quan and R. Li, "A broadband dual-polarized omnidirectional antenna for base stations," *IEEE Trans. Antennas Propag.*, vol. 61, no. 2, pp. 943–947, Feb. 2013.

[3] H. Huang, Y. Liu, and S. Gong, "Broadband dual-polarized omnidirectional antenna for 2G/3G/LTE/WiFi applications," *IEEE Antennas Wireless Propag. Lett.*, vol. 15, pp. 576–579, 2016.

[4] D. Guo, K. He, Y. Zhang, and M. Song, "A multiband dual-polarized omnidirectional antenna for indoor wireless communication systems," *IEEE Antennas Wireless Propag. Lett.*, vol. 16, pp. 290–293, 2017.

[5] H. Wen, Y. Qi, Z. Weng, F. Li, and J. Fan, "A multiband dual-polarized omnidirectional antenna for 2G/3G/LTE application," *IEEE Antennas Wireless Propag. Lett.*, vol. 17, no. 2, pp. 180–183, Feb. 2018.

[6] J. Wang, Z. Shen, and L. Zhao, "Wideband dual-polarized antenna for spectrum monitoring systems," *IEEE Antennas Wireless Propag. Lett.*, vol. 16, pp. 2236–2239, 2017.

[7] J. Wang, L. Zhao, Z.-C. Hao, and J.-M. Jin, "A wideband dual-polarized omnidirectional antenna for base station/WLAN," *IEEE Trans. Antennas Propag.*, vol. 66, no. 1, pp. 81–87, Jan. 2018.

[8] Y. Fan, X. Liu, B. Liu, and R. Li, "A broadband dual-polarized omnidirectional antenna based on orthogonal dipoles," *IEEE Antennas Wireless Propag. Lett.*, vol. 15, pp. 1257–1260, 2016.

[9] J. Wu, S. Yang, Y. Chen, S. W. Qu, and Z. Nie, "A low profile dual-polarized wideband omnidirectional antenna based on AMC reflector," *IEEE Trans. Antennas Propag.*, vol. 65, no. 1, pp. 368–374, Jan. 2017.

[10] Y. Li, Z. Zhang, J. Zheng, and Z. Feng, "Compact azimuthal omnidirectional dual-polarized antenna using highly isolated colocated slots," *IEEE Trans. Antennas Propag.*, vol. 60, no. 9, pp. 4037–4045, Sep. 2012.

[11] Y. Li, Z. Zhang, Z. Feng, and M. F. Iskander, "Design of omnidirectional dual-polarized antenna in slender and low-profile column," *IEEE Trans. Antennas Propag.*, vol. 62, no. 4, pp. 2323–2326, Apr. 2014.

[12] P. Liu, Y. Li, Z. Zhang, and Z. Feng, "Omnidirectional dual-polarized antenna with sabre-like structure," *IEEE Trans. Antennas Propag.*, vol. 65, no. 6, pp. 3221–3225, Jun. 2017.

[13] C. Deng, P. Li, and W. Cao, "A high-isolation dual-polarization patch antenna with omnidirectional radiation patterns," *IEEE Antennas Wireless Propag. Lett.*, vol. 11, pp. 1273–1276, 2012.

[14] Y. Liu, J. Xue, H. Wang, and S. Gong, "Low-profile omnidirectional dual-polarised antenna for 2.4 GHz WLAN applications," *Electron. Lett.*, vol. 50, no. 14, pp. 975–976, Jul. 2014.

[15] A. C. K. Mak, C. R. Rowell, and R. D. Murch, "Isolation enhancement between two closely packed antennas," *IEEE Trans. Antennas Propag.*, vol. 56, no. 11, pp. 3411–3419, Nov. 2008.

[16] S. Zhang, B. K. Lau, Y. Tan, Z. Ying, and S. He, "Mutual coupling reduction of two PIFAs with a T-shape slot impedance transformer for MIMO mobile terminal," *IEEE Trans. Antennas Propag.*, vol. 60, no. 3, pp. 1521–1531, Mar. 2012.

[17] F. Yang and Y. Rahmat-Samii, "Microstrip antennas integrated with electromagnetic band-gap (EBG) structures: A low mutual coupling design for array applications," *IEEE Trans. Antennas Propag.*, vol. 51, no. 10, pp. 2936–2946, Oct. 2003.

[18] A. Diallo, C. Luxey, P. Le Thuc, R. Staraj, and G. Kossiavas, "Study and reduction of the mutual coupling between two mobile phone PIFAs operating in the DCS1800 and UMTS bands," *IEEE Trans. Antennas Propag.*, vol. 54, no. 11, pp. 3063–3073, Nov. 2006.

[19] S. Saxena, B. K. Kanaujia, S. Dwari, S. Kumar, and R. Tiwari, "MIMO antenna with built-in circular shaped isolator for sub-6 GHz 5G applications," *Electron. Lett.*, vol. 54, no. 8, pp. 478–480, Apr. 2018.

[20] K. Saurav, N. K. Mallat, and Y. M. M. Antar, "A three-port polarization and pattern diversity ring antenna," *IEEE Antennas Wireless Propag. Lett.*, vol. 17, no. 7, pp. 1324–1328, Jul. 2018.

[21] K. Wei, Z. Zhang, W. Chen, and Z. Feng, "A novel hybrid-fed patch antenna with pattern diversity," *IEEE Antennas Wireless Propag. Lett.*, vol. 9, pp. 562–565, 2010.

[22] C. Deng, Y. Li, X. Lv, and Z. Feng, "Wideband dual-mode patch antenna with compact CPW feeding network for pattern diversity application," *IEEE Trans. Antennas Propag.*, vol. 66, no. 5, pp. 2628–2633, May 2018.

[23] X. Liu, Y. Wu, Z. Zhuang, W. Wang, and Y. Liu, "A dual-band patch antenna for pattern diversity application," *IEEE Access*, vol. 6, pp. 51986–51993, 2018.

[24] Y. Zhang, K. Wei, Z. Zhang, Y. Li, and Z. Feng, "A compact dual-mode metamaterial-based loop antenna for pattern diversity," *IEEE Antennas Wireless Propag. Lett.*, vol. 14, pp. 394–397, 2015.

[25] L. Cui, W. Wu, and D. G. Fang, "Wideband circular patch antenna for pattern diversity application," *IEEE Antennas Wireless Propag. Lett.*, vol. 14, pp. 1298–1301, 2015.

[26] W. K. Toh, Z. N. Chen, X. Qing, and T. S. P. See, "A planar UWB diversity antenna," *IEEE Trans. Antennas Propag.*, vol. 57, no. 11, pp. 3467–3473, Nov. 2009.

[27] T. K. Roshna, U. Deepak, and P. Mohanan, "Compact UWB MIMO antenna for tridirectional pattern diversity characteristics," *IET Microw., Antennas Propag.*, vol. 11, no. 14, pp. 2059–2065, 2017.

[28] Y. Li, Z. Zhang, J. Zheng, Z. Feng, and M. F. Iskander, "Experimental analysis of a wideband pattern diversity antenna with compact reconfigurable CPW-to-slotline transition feed," *IEEE Trans. Antennas Propag.*, vol. 59, no. 11, pp. 4222–4228, Nov. 2011.

[29] H. T. Chattha, Y. Huang, S. J. Boyes, and X. Zhu, "Polarization and pattern diversity-based dual-feed planar inverted-F antenna," *IEEE Trans. Antennas Propag.*, vol. 60, no. 3, pp. 1532–1539, Mar. 2012.

[30] Y. Dong, J. Choi, and T. Itoh, "Vivaldi antenna with pattern diversity for 0.7 to 2.7 GHz cellular band applications," *IEEE Antennas Wireless Propag. Lett.*, vol. 17, no. 2, pp. 247–250, Feb. 2018.

[31] D. Sarkar, K. Saurav, and K. V. Srivastava, " Dual band complementary split-ring resonator-loaded printed dipole antenna arrays for pattern diversity multiple-input–multiple-output applications," *IET Microw., Antennas Propag.*, vol. 10, no. 10, pp. 1113–1123, 2016.

[32] J. Hu and Z.-C. Hao, "A compact polarization-reconfigurable and 2-D beam-switchable antenna using the spatial phase shift technique," *IEEE Trans. Antennas Propag.*, vol. 66, no. 10, pp. 4986–4995, Oct. 2018.

[33] B. Chiang and M. Holdip, "Progressively phased circular arrays used in antenna isolation," in *Proc. IEEE Antennas Propag. Soc. Int. Symp.*, Jun. 1974, pp. 289–292.

[34] K. E. Kolodziej, P. T. Hurst, A. J. Fenn, and L. I. Parad, "Ring array antenna with optimized beamformer for simultaneous transmit and receive," in *Proc. IEEE Int. Symp. Antennas Propag.*, Jul. 2012, pp. 1–2.

[35] E. A. Etellisi, M. A. Elmansouri, and D. S. Filipović, "Wideband simultaneous transmit and receive (STAR) circular array system," in *Proc. IEEE Int. Symp. Phased Array Syst. Technol.*, Waltham, MA, USA, Oct. 2016, pp. 1–5.

[36] R. Lian, T.-Y. Shih, Y. Yin, and N. Behdad, "A high-isolation, ultra-wideband simultaneous transmit and receive antenna with monopole-like radiation characteristics," *IEEE Trans. Antennas Propag.*, vol. 66, no. 2, pp. 1002–1007, Feb. 2018.
[37] R. G. Vaughan and J. B. Andersen, "Antenna diversity in mobile communications," *IEEE Trans. Veh. Technol.*, vol. VT-36, no. 4, pp. 147–172, Nov. 1987.
[38] J. Huang, "A technique for an array to generate circular polarization with linearly polarized elements," *IEEE Trans. Antennas Propag.*, vol. AP-34, no. 9, pp. 1113–1124, Sep. 1986.
[39] J. D. Kraus and R. J. Marhefka, *Antennas*, 3rd ed. New York, NY, USA: McGrawHill, 2001.
[40] W. Liu, Z. Zhang, Z. Feng, and M. Iskander, "A compact wideband microstrip crossover," *IEEE Microw. Wireless Compon. Lett.*, vol. 22, no. 5, pp. 254–256, May 2012.

Libin Sun received the B.S. degree from Xidian University, Xi'an, China, in 2016. He is currently pursuing the Ph.D. degree in electrical engineering with Tsinghua University, Beijing, China.

His current research interests include antenna design and theory, particularly in mobile phone antennas, MIMO and diversity antennas, circularly polarized antennas, leaky-wave antennas, surface wave antennas, and stretchable and flexible antennas.

Mr. Sun serves as a reviewer for the IEEE TRANSACTIONS ON ANTENNAS AND PROPAGATION and IEEE ANTENNAS AND WIRELESS PROPAGATION LETTERS.

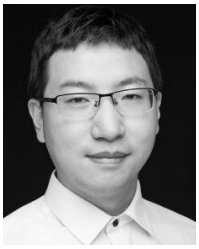

Yue Li (S'11–M'12–SM'17) received the B.S. degree in telecommunication engineering from Zhejiang University, Hangzhou, Zhejiang, China, in 2007, and the Ph.D. degree in electronic engineering from Tsinghua University, Beijing, China, in 2012.

In 2012, he joined the Department of Electronic Engineering, Tsinghua University, as a Post-Doctoral Fellow. In 2013, he joined the Department of Electrical and Systems Engineering, University of Pennsylvania, Philadelphia, PA, USA, as a Research Scholar. In 2010, he was a Visiting Scholar with the Institute for Infocomm Research, A∗STAR, Singapore, and the Hawaii Center of Advanced Communication, University of Hawai'i at Mānoa, Honolulu, HI, USA, in 2012. Since 2016, he has been with Tsinghua University, where he is currently an Associate Professor with the Department of Electronic Engineering. He has authored and co-authored over 100 journal papers and 40 international conference papers. He holds 17 granted Chinese patents. His current research interests include metamaterials, plasmonics, electromagnetics, nanocircuits, mobile and handset antennas, MIMO and diversity antennas, and millimeter-wave antennas and arrays.

Dr. Li was a recipient of the Issac Koga Gold Medal from URSI General Assembly in 2017, the Second Prize of Science and Technology Award of China Institute of Communications in 2017, the Young Scientist Awards from the conferences of ACES 2018, AT-RASC 2018, AP-RASC 2016, EMTS 2016, and URSI GASS 2014, the best paper awards from the conferences of CSQRWC 2018, NCMMW 2018 and 2017, APCAP 2017, NCANT 2017, ISAPE 2016, and ICMMT 2016, the Outstanding Doctoral Dissertation of Beijing Municipality in 2013, and the Principal Scholarship of Tsinghua University in 2011. He is serving as an Associate Editor for the IEEE TRANSACTIONS ON ANTENNAS AND PROPAGATION, IEEE ANTENNAS AND WIRELESS PROPAGATION LETTERS, and Computer Applications in Engineering Education. He is on the Editorial Board of *Scientific Report.*

Zhijun Zhang (M'00–SM'04–F'15) received the B.S. and M.S. degrees from the University of Electronic Science and Technology of China, Chengdu, China, in 1992 and 1995, respectively, and the Ph.D. degree from Tsinghua University, Beijing, China, in 1999.

In 1999, he joined the Department of Electrical Engineering, University of Utah, Salt Lake City, UT, USA, as a Post-Doctoral Fellow, where he was appointed as a Research Assistant Professor in 2001. In 2002, he joined the University of Hawai'i at Mānoa, Honolulu, HI, USA, as an Assistant Researcher. In 2002, he joined Amphenol T&M Antennas, Vernon Hills, IL, USA, as a Senior Staff Antenna Development Engineer, where he was promoted to the position of Antenna Engineer Manager. In 2004, he joined Nokia Inc., San Diego, CA, USA, as a Senior Antenna Design Engineer. In 2006, he joined Apple Inc., Cupertino, CA, as a Senior Antenna Design Engineer, where he was promoted to the position of Principal Antenna Engineer. Since 2007, he has been with Tsinghua University, where he is currently a Professor with the Department of Electronic Engineering. He has authored *Antenna Design for Mobile Devices* (Wiley, 1st ed., 2011, 2nd ed., 2017).

Dr. Zhang served as an Associate Editor for the IEEE TRANSACTIONS ON ANTENNAS AND PROPAGATION from 2010 to 2014 and IEEE ANTENNAS AND WIRELESS PROPAGATION LETTERS from 2009 to 2015.

Magdy F. Iskander (F'93–LF'12) was a Professor of electrical and computer engineering and the Engineering Clinic Endowed Chair Professor with the University of Utah, Salt Lake City, UT, USA. In 2002, he joined the University of Hawai'i at Mānoa, Honolulu, HI, USA, where he is currently a Professor of electrical engineering and the Director of the Hawaii Center for Advanced Communications, College of Engineering. He is also the Co-Director of the NSF Industry/University Co-Operative Research Center, Honolulu, HI, USA, with four other universities. He has authored over 250 papers in technical journals and authored and edited several books, including the textbook *Electromagnetic Fields and Waves* (Prentice Hall, 1992, and Waveland Press, 2001; 2nd ed., 2012), and four books published by the Materials Research Society on Microwave Processing of Materials. He holds nine patents and has made numerous presentations at national/international conferences. His current research interests include computational and biomedical electromagnetics and wireless communications that were funded by the National Science Foundation, National Institute of Health, Army Research Office, U.S. Army CERDEC, Office of Naval Research, and several corporate sponsors.

Mr. Iskander was the President of the IEEE Antennas and Propagation Society in 2002, a Distinguished Lecturer, and a Program Director of the Electrical, Communications, and Cyber Systems Division at the National Science Foundation. He was a recipient of many awards for excellence in research and teaching, including the University of Hawaii Board of Regents' Medal for Excellence in Research in 2013, the Board of Regents Medal for Teaching Excellence in 2010, the Hi Chang Chai Outstanding Teaching Award in 2011 and 2014, which is based on votes by graduating seniors, the IEEE MTT-S Distinguished Educator Award in 2013, the IEEE AP-S Chen-To Tai Distinguished Educator Award in 2012, the Richard R. Stoddard Award from the IEEE EMC Society in 1992, the Northrop Grumman Excellence in Teaching Award in 2010, the American Society for Engineering Education Curtis W. McGraw National Research Award in 1985, and the ASEE George Westinghouse National Award for Excellence in Education in 1991. He has been the Founding Editor of the *Computer Applications in Engineering Education Journal* since 1992.